Chinese Physics Letters

LETTER

Modeling Bacterial Flow Field with Regularized Singularities

To cite this article: Yaochen Yang *et al* 2026 *Chinese Phys. Lett.* **43** 050901

View the article online for updates and enhancements.

You may also like

- Correlation properties of collective motion in bacterial suspensions
Shawn D Ryan, Andrey Sokolov, Leonid Berlyand et al.
- Flow structure around a microswimmer at fluid–fluid interface
Rishish Mishra, Mounika Gosika, Harinadha Gidituri et al.
- Propulsive matrix of a helical flagellum
He-Peng Zhang, , Bin Liu et al.

This content was downloaded from IP address 159.226.35.236 on 09/05/2026 at 03:06

Modeling Bacterial Flow Field with Regularized Singularities

Yaochen Yang[1,2], Daiki Matsunaga[3*], Da Wei[4*], and Fanlong Meng[1,2,5*]

[1]*Institute of Theoretical Physics, Chinese Academy of Sciences, Beijing 100190, China*
[2]*School of Physical Sciences, University of Chinese Academy of Sciences, Beijing 100049, China*
[3]*Graduate School of Engineering Science, The University of Osaka, Toyonaka 5608531, Japan*
[4]*Beijing National Laboratory for Condensed Matter Physics, Institute of Physics, Chinese Academy of Sciences, Beijing 100190, China*
[5]*Wenzhou Institute, University of Chinese Academy of Sciences, Wenzhou 325000, China*

(Received 6 February 2026; accepted manuscript online 24 March 2026)

The flow field generated by a swimming bacterium serves as a fundamental building block for understanding hydrodynamic interactions between bacteria. Although the flow field generated by a force dipole (stresslet) well captures the fluid motion in the far field limit, the stresslet description does not work in the near-field limit, which can be important in microswimmer interactions. Here we propose the model combining an anisotropically regularized stresslet with an isotropically regularized source dipole, and it nicely reproduces the flow field around a swimming bacterium, which is validated by the experimental measurements of the flow field around *E. coli* and our boundary-element-method simulations of a helical microswimmer, in both cases of the free space and the confined space with a no-slip wall. This work provides a practical tool for obtaining the flow field of the bacterium, and can be utilised to study the collective responses of bacteria in dense suspensions.

DOI: 10.1088/0256-307X/43/5/050901 CSTR: 32039.14.0256-307X.43.5.050901

During the swimming process, a bacterium can generate a flow field in the surrounding fluid, which mediates its interactions with passive particles, other bacteria, etc..[1–5] To formulate this flow field, continuous efforts have been dedicated for decades. In the far field limit, the flow has been well-resolved and described as that generated by a force dipole, i.e., stresslet.[6–8] However, when approaching the cell body of the bacterium, the above stresslet description would fail,[9–11] primarily due to the finite size effect of the cell body,[12,13] and this renders the difficulties in discussing the flow field close to a bacterium and the hydrodynamic interactions between bacteria occurring at close distances.[14–16]

The above-mentioned need to understand the near-field hydrodynamics of bacteria has motivated sustained theoretical attempts,[17–19] where the flow regularization method is taken as a promising candidate. Regularization, a mathematical technique that replaces singular solutions in hydrodynamic computations with smooth analytical functions, prevents the flow field from diverging near the singularity points and facilitates approachable numerical computations.[20] For example, a regularized Stokeslet is usually implemented by replacing the point force, specifically a Dirac delta function, with a smooth function (*blob* function) of certain geometry and characteristic length scale, and it has been widely utilised for modeling ciliary and flagellar flows.[21–24] For the flow field generated by a microswimmer, the description based on regularized singularities remains underexplored. This is partly because the flow field generated by a swimming microorganism—even one as simple as a bacterium—is typically complex, owing to its irregular geometry and intricate swimming mechanism. Despite some initial but meaningful efforts, such as representing the flow field by combining a regularized stresslet and rotlet dipole,[25] until now, these theoretical attempts do not quantitatively capture the experimentally observed near-field flow structure, which is essential for determining bacterial hydrodynamic interaction in dense suspension. Moreover, most of the current regularization methods use isotropic blob functions, which are inherently unable to account for the anisotropy of the bacterial body and to capture the accurate near-body flow.

In this work, we develop an anisotropic regularization scheme to resolve the flow field of a swimming bacterium. By comparing with the experiments in Ref. [10] and our Boundary Element Method (BEM) simulations, we show that the flow field near a swimming *E. coli* bacterium can be accurately described as that generated by an anisotropically regularized stresslet and an isotropically regularized source dipole. This description quantitatively captures the radial flows in both the far-field and near-field limit, and also in both cases of the free space and the confined space with a no-slip wall.

Theoretical Model. Consider a bacterium whose body center is located at the origin and the body axis is oriented along $+x$, as shown in Fig. 1, and then the flow field generated by the bacterium can be modelled as a superposition of the flow fields generated by an anisotropically

*Corresponding authors. Email: daiki.matsunaga.es@osaka-u.ac.jp; weida@iphy.ac.cn; fanlong.meng@itp.ac.cn
© 2026 Chinese Physical Society and IOP Publishing Ltd. All rights, including for text and data mining, AI training, and similar technologies, are reserved.

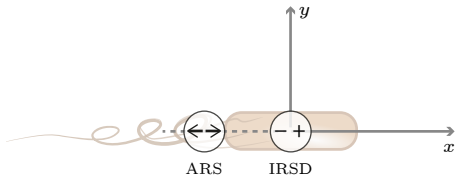


Fig. 1. The theoretical setup, with the ARS (anisotropically regularized stresslet) placed between the cell body and the flagellar bundle, and the IRSD (isotropically regularized source dipole) placed at the center of the cell body. The director of bacterium, $\boldsymbol{q}$, is set along the $+x$.

regularized stresslet (ARS) and an isotropically regularized source dipole (IRSD). Note the anisotropy introduced in ARS can help to characterize the flow field induced by non-spherical shape of the swimmer.

The flow field generated by the ARS, $\boldsymbol{u}^{\mathrm{ARS}}(\boldsymbol{r})$, is constructed as:

$$\boldsymbol{u}^{\mathrm{ARS}}(\boldsymbol{r}) = -\boldsymbol{D} : \nabla G_{\varepsilon,\boldsymbol{q}}(\boldsymbol{r}), \tag{1}$$

where $\boldsymbol{D} = D \cdot \boldsymbol{qq}$ denotes stresslet, and $G_{\varepsilon,\boldsymbol{q}}(\boldsymbol{r})$ denotes the Green function relating the flow field with a regularized Stokeslet, which can be obtained by solving the Stokes equation, $\nabla p - \mu\nabla^2\boldsymbol{u} = \boldsymbol{F} f_{\varepsilon,\boldsymbol{q}}(\boldsymbol{r})$ with p as the pressure, μ the viscosity, $\boldsymbol{F}$ the force, and $f_{\varepsilon,\boldsymbol{q}}(\boldsymbol{r})$ representing the anisotropic Gaussian blob.[18] Specifically, the anisotropic Gaussian blob function, $f_{\varepsilon,\boldsymbol{q}}(\boldsymbol{r})$, is taken as

$$f_{\varepsilon,\boldsymbol{q}}(\boldsymbol{r}) = \frac{1}{\pi\sqrt{\pi}\varepsilon_{\parallel}\varepsilon_{\perp}^2} \exp\Big(-\frac{r_{\parallel}^2}{\varepsilon_{\parallel}^2} - \frac{r_{\perp}^2}{\varepsilon_{\perp}^2}\Big), \tag{2}$$

where the distance $r_{\parallel} = |\boldsymbol{q}\cdot\boldsymbol{r}|$ and $r_{\perp} = |\boldsymbol{r} - r_{\parallel}\boldsymbol{q}|$, and $\varepsilon_{\parallel}$ and $\varepsilon_{\perp}$ are two regularization parameters along and perpendicular to the body axis oriented in the direction $\boldsymbol{q}$, respectively. For a regularized stresslet (located at the origin), the regularization parameters generally correspond to the distance at which the flow velocities $u_x(x,0,0)$ and $u_y(0,y,0)$ reach their extrema along x- and y-axes, respectively [see more details in Supplementary Material (SM)].

Meanwhile, the flow field generated by the isotropically regularized source dipole (IRSD), $\boldsymbol{u}^{\mathrm{IRSD}}(\boldsymbol{r})$, is constructed from a regularized source monopole. The flow field by a source monopole can be expressed in the form of the gradient of a potential function: $\nabla\psi_{\lambda}(\boldsymbol{r})$,[26] with the potential function ψ_{λ} determined by the blob $f_{\lambda}(\boldsymbol{r})$, as $\psi_{\lambda}(\boldsymbol{r}) = -\frac{1}{4\pi}\int \frac{1}{|\boldsymbol{r}-\boldsymbol{r}'|} f_{\lambda}(\boldsymbol{r}')\,\mathrm{d}\boldsymbol{r}'$. By taking the Gaussian blob $f_{\lambda}(\boldsymbol{r}) = \frac{1}{\pi\sqrt{\pi}\lambda^3}\mathrm{e}^{-r^2/\lambda^2}$, we can obtain the analytical form of the potential function,

$$\psi_{\lambda}(\boldsymbol{r}) = -\frac{1}{4\pi r}\mathrm{erf}\Big(\frac{r}{\lambda}\Big). \tag{3}$$

Then the flow field generated by IRSD is given by

$$\boldsymbol{u}^{\mathrm{IRSD}}(\boldsymbol{r}) = -\boldsymbol{d}\cdot\nabla\nabla\psi_{\lambda}(\boldsymbol{r}), \tag{4}$$

where $\boldsymbol{d} = d\cdot\boldsymbol{q}$ denotes the source dipole.

Then, the entire flow field in the laboratory frame is given by the superposition of the above two flow field generated by the ARS and IRSD. For simplicity, we set $\boldsymbol{q}$ as $+x$-direction. Since the center of the cell body is located at the origin and flagellar bundle extends to $x < 0$, ARS center is placed at $\boldsymbol{r}_{\mathrm{A}} = (-l, 0, 0)$, as shown in Fig. 1. Because IRSD enforces no-slip condition at the two ends of the long axis of the cell body, which is symmetric regarding the origin, its center coincides with the geometric center of the cell body. Therefore, the entire flow field is given by

$$\boldsymbol{u}(\boldsymbol{r}) = \boldsymbol{u}^{\mathrm{ARS}}(\boldsymbol{r} - \boldsymbol{r}_{\mathrm{A}}) + \boldsymbol{u}^{\mathrm{IRSD}}(\boldsymbol{r}). \tag{5}$$

Note that since the regularization does not alter the far-field behavior of singularity solutions, the strength of both the stresslet $\boldsymbol{D}$ and the source dipole $\boldsymbol{d}$ are defined in the same fashion as those in the case without regularization. For readers familiar with the squirmer model,[27–30] a higher-order multipole summation is usually needed for accurately capturing the flow field near the cell body, which is computationally heavy.

Comparisons with Experiments and Simulations. We compare the theoretical results obtained by the above model with both the experiments on *E. coli*[10] and our BEM simulations. In BEM simulations, the bacterial body is simplified as a sphere of 1 μm radius and the flagellar bundle is represented by a helical tail of 10 μm length in the swimming direction (x direction), and one can refer to SM for more details. The comparisons are focused on the axial velocity along the $+x$-axis, $u_x(x,0,0)$ ($x > 1\,\mu\mathrm{m}$), and the lateral velocity along the $+y$-axis, $u_y(0,y,0)$ ($y > 1\,\mu\mathrm{m}$), where 1 μm is chosen due to the fact that the size of the cell body in BEM simulations is 1 μm. These velocities are referred to as the *head* and *side* velocities in following discussions, respectively. We shall discuss the flow fields generated by the bacterium in both the free space and the confined space with a no-slip wall.

In the free space, both the experimental and BEM results are accurately captured by the theoretical predictions using the parameter set $\{D = 1\,\mathrm{pN{\cdot}\mu m},\ l = 1.6\,\mu\mathrm{m},\ \varepsilon_{\parallel} = 1\,\mu\mathrm{m},\ \varepsilon_{\perp} = 1.36\,\mu\mathrm{m},\ d = 140\,\mu\mathrm{m}^4/\mathrm{s},\ \lambda = 0.7\,\mu\mathrm{m}\}$. Note that the parameter D and l have explicit physical correspondence, which are the stresslet strength[10,31] and half body length[32–34] of *E. coli*, respectively. Thus, the primary fitting parameters in our system are the regularization lengths of the stresslet, i.e., $\{\varepsilon_{\parallel}, \varepsilon_{\perp}\}$. Since $\varepsilon_{\parallel}$ and $\varepsilon_{\perp}$ are highly coupled, we fix $\varepsilon_{\parallel} = 1\,\mu\mathrm{m}$ and fit only $\varepsilon_{\perp}$ (correlated with the body geometry, see SM) throughout this work. In the secondary fitting step, the IRSD is introduced to better capture the surface flow velocity in the x-direction and to "fine-tune" the region within ∼1 body length from the cell, and the parameters, $\{d, \lambda\}$, are fitted independently. This sequential fitting procedure avoids overfitting of the system.

The pattern of the flow field in the xy-plane, calculated by the model, is provided in Fig. 2(a). In the far field limit, the flow velocity decays in the form of $\propto r^{-2}$ as shown in in Fig. 2(b), same as that by a singular stresslet. This is due to the fast decay of the flow field given by IRSD, which is in the form of $\propto r^{-3}$, and the effect of IRSD then becomes negligble in the far field limit. In the near field limit, the model captures two main features observed

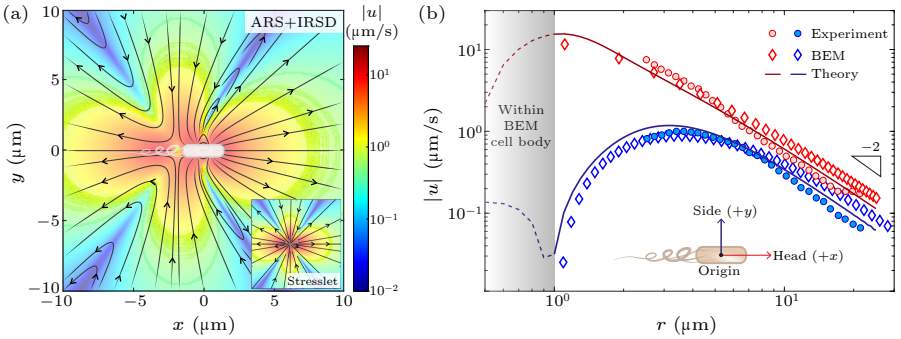


Fig. 2. (a) Entire flow field (ARS + ISRD) given by the model in the free space. Colorbar indicates the magnitude of the in-plane flow velocity $|u| = \sqrt{u_x^2 + u_y^2}$. Flow field of a stresslet of the same strength as the ARS is presented in the inset. ARS: anisotropically regularized stresslet, IRSD: isotropically regularized source dipole. (b) The head and side flow profile $|u_x(x,0,0)|$ (red) and $|u_y(0,y,0)|$ (blue). Experimental measurements are represented by dots, numerical simulations by diamonds. Theoretical predictions inside and outside the BEM cell body surface are shown as dashed and solid lines, respectively. The fluid viscosity, $\mu = 1 \times 10^{-3}$ Pa·s is used in calculations throughout this work.

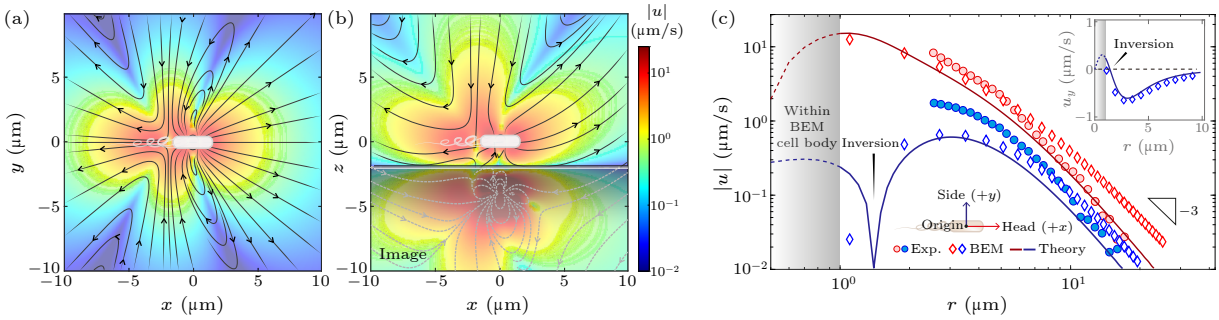


Fig. 3. (a) and (b) Entire flow field given by the model in presence of a no-slip wall. Colorbar shows the magnitude of the in-plane flow velocity: (a) $|u| = \sqrt{u_x^2 + u_y^2}$ and (b) $|u| = \sqrt{u_x^2 + u_z^2}$. (c) The head and side flow profile $|u_x(x,0,0)|$ and $|u_y(0,y,0)|$. Experimental measurements are represented by dots, numerical simulations by diamonds. Theoretical predictions inside and outside the BEM cell body surface are shown as dashed and solid lines, respectively. The inset shows the side flow profile $u_y(0,y,0)$ around the inversion point.

in experiments and BEM simulations: (a) the head flow profile, $u_x(x,0,0)$, decays monotonically and the swimming speed is close to that obtained in BEM simulations, 11.8 μm/s; (b) the side flow profile, $u_y(0,y,0)$, has an initial increase followed by a decrease in the form of $\propto r^{-2}$, and the flow speed approaches zero at the surface $y = 1$ μm, due to the flow inversion induced by the stresslet center offset l.

Then we generalise the comparisons to the case in the confined space with a no-slip wall, where the wall confinement is important in changing the flow field.[35,36] Theoretically, we need to calculate the flow field by considering the wall effect and by considering the contributions of image systems:[37,38]

$$\boldsymbol{u}_{\text{wall}}^{\text{ARS}}(\boldsymbol{r}) = \boldsymbol{u}^{\text{ARS}} + \boldsymbol{u}_{\text{img}}^{\text{ARS}}, \tag{6}$$

$$\boldsymbol{u}_{\text{wall}}^{\text{IRSD}}(\boldsymbol{r}) = \boldsymbol{u}^{\text{IRSD}} + \boldsymbol{u}_{\text{img}}^{\text{IRSD}}. \tag{7}$$

The image system of ARS is derived by anisotropically regularizing the Blake tensor and the image system of IRSD is derived based on the image system of an isotropically regularized source monopole (see SM for more details). To compute the flow field near the wall in BEM simulations, the bacterium is placed above a no-slip wall with the distance 2 μm. All other settings are kept identical to those in the case of the free space.

The flow field parallel to the surface (xy-plane) and perpendicular to the surface (xz-plane) are shown in Figs. 3(a) and 3(b), respectively. The flow profiles along the head and side directions are shown in Fig. 3(c). The flow field in the near field limit behaves similarly to that in the free space, whereas the velocity decaying in the far field limit follows the form of $\propto r^{-3}$ due to the no-slip wall. Note that both the theoretical results and BEM simulations show that the extremum of the side flow profile is lower than that in the free space, whereas the experimental measurements show the opposite trend: the extremum of the side flow profile being higher in the presence of the wall. This discrepancy can originate from a spiral flow field, which is usually described by a pair of opposite rotlets.[1,25,39] Note that when comparing u_y in Fig. 3, we have removed the contribution of the rotlet dipole by taking $u_y(0,y,0) = [u_y'(0,y,0) - u_y'(0,-y,0)]/2$ where u_y' denotes the raw flow field in BEM (see SM).

Summary. We develop an analytical model for describing the flow field generated by a swimming bacterium, in both the far field and the near field limit, based on the combination of regularized singularities. The theoretical results are validated by comparisons with experiments and our BEM simulations. The anisotropy introduced in the model nicely captures the geometry of a bac-

terium, and thus the flow field. The approach provides a complementary view to the multipole expansion of microswimmer flow fields[40,41] and can boost further investigations in flow fields generated by other microorganisms.[9,42,43] Moreover, the flow field predicted by the model can be utilised to describe the hydrodynamic interactions (forces and torques) between bacteria in dense suspensions, which is important in determining the collective dynamics of bacteria, e.g., bacterial turbulence.

Acknowledgements. We thank Knut Drescher for the informational input on interpreting the experimental data, and Ramin Golestanian for discussion. F.M. acknowledges supports by the National Natural Science Foundation of China (NSFC) (Grant Nos. 12275332 and 12447101), Max Planck Society (Max Planck Partner Group), Wenzhou Institute (Grant No. WIUCASQD2023009), Beijing National Laboratory for Condensed Matter Physics (Grant No. 2023BNLCMPKF005), and the UCAS Xiaomi Youth Fellowship. D.W. acknowledges supports by the NSFC (Grant No. 12574238). D.M. acknowledges supports by the Japan Society for the Promotion of Science KAKENHI (Grant Nos. 21H05879, 23K22673, 23H04418, and 23K26040), the Japan Science and Technology Agency PRESTO (Grant No. JP-MJPR21OA), and the JSPS Core-to-Core Program "Advanced core-to-core network for the physics of self-organizing active matter (JPJSCCA20230002)".

References

[1] Lauga E 2016 *Annu. Rev. Fluid Mech.* **48** 105
[2] Purcell E M 1977 *Am. J. Phys.* **45** 3
[3] Berke A P, Turner L, Berg H C, and Lauga E 2008 *Phys. Rev. Lett.* **101** 038102
[4] Koch D L and Subramanian G 2011 *Annu. Rev. Fluid Mech.* **43** 637
[5] Ning L, Lou X, Ma Q, Yang Y, Luo N, Chen K, Meng F, Zhou X, Yang M, and Peng Y 2023 *Phys. Rev. Lett.* **131** 158301
[6] Lauga E and Powers T R 2009 *Rep. Prog. Phys.* **72** 096601
[7] Batchelor G K 1970 *J. Fluid Mech.* **41** 545
[8] Pedley T J and Kessler J O 1992 *Annu. Rev. Fluid Mech.* **24** 313
[9] Drescher K, Goldstein R E, Michel N, Polin M, and Tuval I 2010 *Phys. Rev. Lett.* **105** 168101
[10] Drescher K, Dunkel J, Cisneros L H, Ganguly S, and Goldstein R E 2011 *Proc. Natl. Acad. Sci. U.S.A.* **108** 10940
[11] Zhang B, Leishangthem P, Ding Y, and Xu X 2021 *Proc. Natl. Acad. Sci. U.S.A.* **118** e2100145118
[12] Wei D, Hu S, Tang T, Yang Y, Meng F, and Peng Y 2025 *Phys. Rev. Lett.* **135** 188401
[13] Kamdar S, Shin S, Leishangthem P, Francis L F, Xu X, and Cheng X 2022 *Nature* **603** 819
[14] Gautam D, Meena H, Matheshwaran S, and Chandran S 2024 *Phys. Rev. E* **110** L012601
[15] Ishikawa T, Sekiya G, Imai Y, and Yamaguchi T 2007 *Biophys. J.* **93** 2217
[16] Wensink H H, Dunkel J, Heidenreichd S, Drescher K, Goldstein R E, Löwen H, and Yeomans J M 2012 *Proc. Natl. Acad. Sci. U.S.A.* **109** 14308
[17] Cortez R 2001 *SIAM J. Sci. Comput.* **23** 1204
[18] Zhao B, Lauga E, and Koens L 2019 *Phys. Rev. Fluids* **4** 084104
[19] Ainley J, Durkin S, Embid R, Boindala P, and Cortez R 2008 *J. Comput. Phys.* **227** 4600
[20] Smith D J 2018 *J. Comput. Phys.* **358** 88
[21] Cortez R and Nicholas M 2012 *Commun. Appl. Math. Comput. Sci.* **7** 33
[22] Cortez R 2018 *J. Comput. Phys.* **375** 783
[23] Smith D J 2009 *Proc. R. Soc. A* **465** 3605
[24] Zhao B and Koens L 2021 *Fluids* **6** 335
[25] Ishimoto K, Gaffney E A, and Walker B J 2020 *Phys. Rev. Fluids* **5** 093101
[26] Pozrikidis C 2009 *Fluid Dynamics Theory, Computation, and Numerical Simulation* (Springer)
[27] Ishikawa T 2024 *Annu. Rev. Fluid Mech.* **56** 119
[28] Ishimoto K 2013 *Phys. Rev. E* **88** 062702
[29] Graaf J, Mathijssen A J T M, Fabritius M, Menke H, Holm C, and Shendruk T N 2013 *Soft Matter* **12** 4704
[30] Lintuvuori J S, Brown A T, Stratford K, and Marenduzzo D 2013 *Soft Matter* **12** 7959
[31] Hu J, Yang M, Gompper G, and Winkler R G 2015 *Soft Matter* **11** 7867
[32] Linek J S, Arlt J, Jepson A, Dawson T V A, Miroli D, Pilizota T, Martinez V A, and Poon W C K 2016 *Colloids Surf. B* **137** 2
[33] Chattopadhyay S, Moldovan R, Yeung C, and Wu X L 2006 *Proc. Natl. Acad. Sci. U.S.A.* **103** 13712
[34] Wei D, Yang Y, Wei X, Golestanian R, Li M, Meng F, and Peng Y 2024 *Adv. Sci.* **11** 240264
[35] Meng F, Bennett R R, Uchida N, and Golestanian R 2021 *Proc. Natl. Acad. Sci. U.S.A.* **118** e2102828118
[36] Cheng Z, Vilfan A, Wang Y, Golestanian R, and Meng F 2024 *J. R. Soc. Interface* **21** 20240221
[37] Blake J R 1971 *Proc. Camb. Phil. Soc.* **70** 303
[38] Cortez R and Varela D 2015 *J. Comp. Phys.* **285** 41
[39] Lopez D and Lauga E 2014 *Phys. Fluids* **26** 071902
[40] Chwang A T and Wu T Y 1975 *J. Fluid Mech.* **67** 787
[41] Lighthill J 1975 *Mathematical Biofluiddynamics* (Society for Industrial and Applied Mathematics)
[42] Wei D, Dehnavi P G, Aubin-Tam M E, and Tam D 2019 *Phys. Rev. Lett.* **122** 124502
[43] Wei D, Dehnavi P G, Aubin-Tam M E, and Tam D 2021 *J. Fluid Mech.* **915** A70